van Hooff T, Blocken B, Defraeye T, Carmeliet J, van Heijst GJF, 2012. PIV measurements and analysis of transitional flow in a reduced-scale model: ventilation by a free plane jet with Coanda effect. ***Building and Environment*** *56: 301-313.*

PIV measurements and analysis of transitional flow in a reduced-scale model: ventilation by a free plane jet with Coanda effect

T. van Hooff [a,b 1], B. Blocken [a], T. Defraeye [b,c], J. Carmeliet [d,e], G.J.F. van Heijst [f]

[a]Building Physics and Services, Eindhoven University of Technology, P.O. Box 513, 5600 MB Eindhoven, The Netherlands.
[b]Division of Building Physics, Katholieke Universiteit Leuven, Kasteelpark Arenberg 40, P.O. Box 2447, 3001 Leuven, Belgium.
[c]VCBT / MeBioS, Department of Biosystems, Katholieke Universiteit Leuven, Willem de Croylaan 42, P.O. Box 2428, 3001 Leuven, Belgium.
[d]Building Physics, Swiss Federal Institute of Technology Zürich (ETH), Wolfgang-Pauli-Strasse 15, 8093 Zürich, Switzerland.
[e]Laboratory for Building Science and Technology, Swiss Federal Laboratories for Materials Testing and Research (Empa), Überlandstrasse 129, 8600 Dübendorf, Switzerland.
[f]Fluid Dynamics Laboratory, Eindhoven University of Technology, P.O. Box 513, 5600 MB Eindhoven, The Netherlands.

Graphical abstract

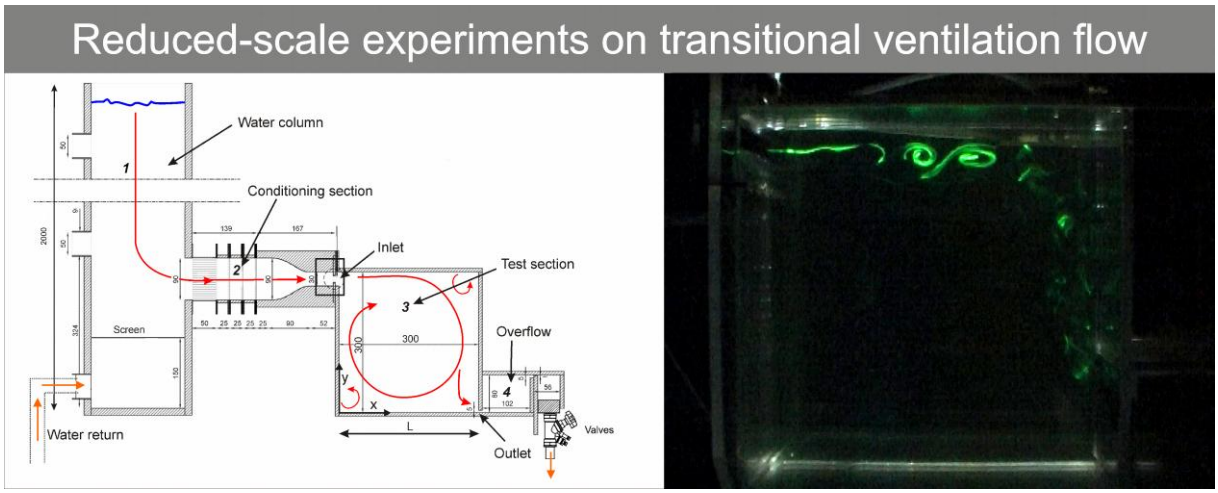

Highlights

- An experimental analysis of flow in a ventilated enclosure has been conducted
- Isothermal forced mixing ventilation flow is driven by a transitional plane jet
- Flow visualizations and PIV measurements performed in a reduced-scale water-filled model
- Slot Reynolds numbers ranging from 800 to 2,500
- Experimental data for the development and validation of CFD models for indoor flow

[1] Corresponding author: E-mail address: t.a.j.v.hooff@tue.nl. Tel.: +31 (0) 40 247 5877; fax: +31 (0) 40 243 8595.

van Hooff T, Blocken B, Defraeye T, Carmeliet J, van Heijst GJF, 2012. PIV measurements and analysis of transitional flow in a reduced-scale model: ventilation by a free plane jet with Coanda effect. ***Building and Environment*** *56: 301-313.*

PIV measurements and analysis of transitional flow in a reduced-scale model: ventilation by a free plane jet with Coanda effect

T. van Hooff [a,b 2], B. Blocken [a], T. Defraeye [b,c], J. Carmeliet [d,e], G.J.F. van Heijst [f]

[a]Building Physics and Services, Eindhoven University of Technology, P.O. Box 513, 5600 MB Eindhoven, The Netherlands.
[b]Division of Building Physics, Katholieke Universiteit Leuven, Kasteelpark Arenberg 40, P.O. Box 2447, 3001 Leuven, Belgium.
[c]VCBT / MeBioS, Department of Biosystems, Katholieke Universiteit Leuven, Willem de Croylaan 42, P.O. Box 2428, 3001 Leuven, Belgium.
[d]Building Physics, Swiss Federal Institute of Technology Zürich (ETH), Wolfgang-Pauli-Strasse 15, 8093 Zürich, Switzerland.
[e]Laboratory for Building Science and Technology, Swiss Federal Laboratories for Materials Testing and Research (Empa), Überlandstrasse 129, 8600 Dübendorf, Switzerland.
[f]Fluid Dynamics Laboratory, Eindhoven University of Technology, P.O. Box 513, 5600 MB Eindhoven, The Netherlands.

Abstract

Knowledge of indoor ventilation airflow is essential for creating a healthy, comfortable and energy-efficient indoor climate in buildings, airplanes, cars, ships, etc. In the past decades, numerical methods such as Computational Fluid Dynamics (CFD) have become primary tools to assess indoor airflow. However, validation of numerical simulations by high-quality experimental data is imperative. Although a lot of studies have focused on experimental data for turbulent ventilation flow, there is a lack of experimental data for transitional ventilation flow. Transitional ventilation flow is in general associated with relatively low air velocities inside the enclosure. This paper presents detailed Particle Image Velocimetry (PIV) measurements and an analysis of transitional flow in a ventilated enclosure. The isothermal forced mixing ventilation flow is driven by a transitional plane jet. The measurements are performed in a reduced-scale water-filled model for slot Reynolds numbers ranging from 800 to 2,500. Flow visualizations indicate that this range of Reynolds numbers results in transitional flow, including the development of large coherent structures in the outer region of the jet. The measurements are analyzed in terms of mean velocity near the inlet and in the entire flow domain, and in terms of turbulence intensity and vorticity. Specific attention is given to the Coanda effect by which the free plane jet develops into a wall jet. The experimental data and analysis are specifically intended to support the development and validation of numerical models for ventilation flow.

Keywords: transitional flow; enclosed space; forced mixing ventilation; Particle Image Velocimetry (PIV); model validation; Coanda effect

1. Introduction

The accurate prediction of ventilation flow is important for creating a healthy, comfortable, sustainable and energy-efficient indoor climate in buildings, airplanes, cars, ships, etc., by removing pollutants, excess heat and moisture and, in extreme cases, fire, smoke and biochemical species. An extensive overview of methods for ventilation studies in rooms or other types of enclosures has been provided by Chen [1]. These methods are: analytical models (e.g. [2-4]), empirical models (e.g. [5-8]), reduced-scale experiments (e.g. [6,9-18]), full-scale experiments (e.g. [19-26]), multizone network models (e.g. [27-29]), zonal models (e.g. [30-33]) and Computational Fluid Dynamics (CFD) (e.g. [4,7,9,10,12,14,17,20-25,34-51]). Chen [1] discussed all seven methods with their potential and shortcomings. Since the early work of Nielsen [9] in the 1970s, the use of CFD to assess indoor airflow has increased tremendously (e.g. [1,51]). Nowadays, it is a primary method for

[2] Corresponding author: E-mail address: t.a.j.v.hooff@tue.nl. Tel.: +31 (0) 40 247 5877; fax: +31 (0) 40 243 8595.

assessing indoor airflow in buildings and other enclosures (e.g. [1,34-51]). Best practice guidelines for CFD in industrial engineering [52-60] and overview publications of room airflow modeling [1,51,61] stipulate the importance of model validation by comparison of the numerical results with the results of full-scale or reduced-scale experiments. Model validation should ensure a proper representation of the reality by the used CFD model [52].

Although reduced-scale experiments can suffer from scaling problems associated with combined modeling of inertial and buoyancy forces, they also have several major advantages, such as the lower cost and the more straightforward application of Particle Image Velocimetry (PIV) compared to full-scale experiments. PIV indeed enables the collection of high-quality data in the reduced-scale set-up, which is less straightforward in a full-scale set-up due to the large field of view that is required [1].

The most commonly applied ventilation methods are displacement ventilation and mixing ventilation. Whereas displacement ventilation consists of injecting the air with relatively low velocities in the lower part of the room, mixing ventilation is based on the injection of an air jet in the upper part of the room [62,63]. The momentum of the jet should ensure mixing of the fresh supply air with the room air, and the diluted air should subsequently be extracted from the room. Attachment of the jet to the ceiling, also known as the 'Coanda effect', is used to ensure that the supply air does not enter the occupant zone too early and helps preventing discomfort for the room occupants [62,64]. Several experimental studies have been conducted in the past to analyze the flow pattern associated with forced mixing ventilation. However, the vast majority of these ventilation studies focused on slot Reynolds numbers (Re) that are considered to be within the turbulent regime (e.g. [10,19,47-50]). The slot Reynolds number, based on the inlet height, can be defined as $Re = (U_0 h)/\nu$ with U_0 the characteristic inlet velocity (m/s), h the slot height (m) and ν the kinematic viscosity (m^2/s). Low values of Re can indicate the presence of a transitional flow regime inside the room, which can be distinguished from turbulent flow by the presence of relatively large coherent structures (vortices). Several publications [22,23,51,61,63,65-67] have indicated the fact that transitional flow can be present in different types of room airflow, either in the supply jet region or in other regions of low velocities (e.g. corners of the room, vicinity of buoyant plumes). The aforementioned studies have indicated the importance of transitional flow in general, and the modeling of transitional flow in room airflow studies in particular. However, to the knowledge of the authors, only a limited number of studies has dealt with room airflow at transitional slot Reynolds numbers so far, either experimentally or numerically. These are briefly discussed below.

Nielsen et al. [65], Topp et al. [66] and Davidson et al. [67] performed measurements and numerical simulations of forced mixing ventilation at transitional slot Reynolds numbers. The measurements of room airflow resulting from a plane wall jet were performed using hot-sphere anemometers at low Reynolds numbers ($Re \approx 79$-770). The depth of the enclosure was 4.2 m; the inlet height was limited to 0.02 m. From their measurements they concluded that the velocity profiles fitted neither a laminar nor a turbulent relation and the flow could thus be regarded as transitional. Wang and Chen [22,23] performed point measurements of airflow in a simplified model of an airline cabin using hot-sphere and ultrasonic anemometers. Their measurements were conducted for $Re = 2{,}600$, which was reported to result in transitional flow. However, in contrast to the experiments in the present paper, the wall jet in their study was fully turbulent, while the transitional flow regime was present in other areas of the enclosure. The main objective of their measurements was to create benchmark data to validate CFD simulations. Van Hooff et al. [68] performed PIV measurements of a transitional wall jet in an enclosure. Their primary aim was to analyze the flow properties of the jet for a range of transitional Re-values.

This paper presents PIV measurements and an analysis of isothermal forced mixing ventilation in a cubical enclosure driven by a transitional plane jet. The study is motivated by the fact that most experimental forced mixing ventilation studies in the past have been conducted for values of Re that are considered to be within the turbulent regime. To the knowledge of the authors, experimental studies on transitional indoor airflow are scarce. As opposed to our previous study [68], the present study focuses on a jet that is injected at a distance from the ceiling (not as a wall jet), which allows investigating the Coanda-effect. In addition, this study is specifically intended to provide experimental data for the development and validation of numerical models. First, the experimental set-up is described in section 2. In section 3, flow visualizations are used to demonstrate the presence of transitional flow for the experiments in this paper. A description of the PIV measurement set-up is given in section 4, after which the results of the PIV measurements are shown and analyzed in section 5. A discussion (section 6) and conclusions (section 7) conclude the paper.

2. Experimental reduced-sale set-up

A reduced-scale model (1:6.67) of an existing 2 x 2 x 2 m^3 air-filled enclosure has been built to perform flow visualizations and PIV measurements of forced mixing ventilation. The reduced-scale experimental set-up is operated with water as fluid medium for purposes of dynamic similarity (Re). It consists of (Fig. 1): (1) a water

column to drive the flow by hydrostatic pressure; (2) a flow conditioning section; (3) a cubic test section with dimensions 0.3 x 0.3 x 0.3 m^3 (L^3); and (4) an overflow. The conditioning section in front of the inlet consists of one honeycomb, three screens and a contraction to minimize the turbulence level at the inlet. The hexagonal honeycombs (type ECM 4.8/77) have a diameter d_h of 4.8 mm and reduce the lateral components of mean velocity, the lateral turbulence intensities and the larger turbulent eddies. The length to diameter ratio of the honeycomb is 10.4 (L_h = 50 mm) (Fig. 2a,b). To reduce the longitudinal components of turbulence and the mean-velocity gradients, three screens are positioned between the honeycombs and the contraction. Bradshaw [69] stated that the porosity should be larger than 57% to optimally reduce the turbulence. The three screens have porosities of 72%, 65% and 60%, and thread diameters of 1.6 mm, 1.0 mm and 0.4 mm, respectively. The screen porosity reduces towards the inlet in order to achieve the lowest level of turbulence [70]. The contraction further reduces the velocity gradients and turbulence intensities by accelerating the flow (Fig. 2c,d). The shape of the contraction is based on the fifth-order polynomial of Bell and Mehta [71], which has been optimized by Brassard and Ferchichi [72] by adding the coefficient α:

$$\xi = \frac{x}{L_c} \tag{1}$$

$$h_g = \left[-10 \cdot \xi^3 + 15 \cdot \xi^4 - 6 \cdot \xi^5 \cdot H_i^{1/\alpha} - H_e^{1/\alpha} + H_i^{1/\alpha} \right]^{\alpha} \tag{2}$$

with ξ the normalized length of the contraction, h_g the normalized height of the contraction, L_c the length of the contraction and H_i and H_e the heights of the contraction inlet and the contraction outlet, respectively, as indicated in Figure 2c. The length L_c of the contraction is 0.09 m, H_e is 0.03 m and H_i is 0.09 m. Defraeye [73] found an optimum value for α of 0.5 based on CFD simulations, resulting in flow acceleration in the contraction without inducing flow separation.

The overflow behind the test section is fitted with a block containing two STAD TA20 balancing valves (Fig. 1), enabling a step-wise adjustment of the volume flow rate through the test section. The 2 m high rectangular construction containing the water column is provided with inlet openings every 0.146 m to be able to vary the static pressure imposed by the water column. Inside this construction a screen has been added to limit the turbulence caused by the insertion of return water. The test section has edges of 0.3 m (L) and is constructed from glass plates with a thickness of 8 mm (Fig. 3a).

Dimensionless coordinates are obtained using the characteristic dimension of the test section L (Fig. 3a) (x/L, y/L, z/L). The inlet width (w_i) is 0.3 m (w_i/L = 1) and the dimensionless inlet height (= h/L) can be varied from 0 to 0.1. For this study h/L is fixed at 0.067 (h = 20 mm). The top edge of the inlet is located at 5 mm from the top surface (y/L = 0.9833). The height of the outlet is fixed at h_{outlet}/L = 0.0167 (h_{outlet} = 5 mm). The slot Reynolds number is defined based on the inlet height as Re_{slot} = Re = U_0h/ν, with U_0 the area-averaged inlet velocity based on the volume flow rate through the inlet and ν the kinematic viscosity at room temperature (≈ 20°C). The maximum local velocity U_M (Fig. 3b) is used to make the velocities non-dimensional (U/U_M). Note that U_M is defined as the local maximum time-averaged x-velocity, and thus varies with both x/L and Re. The distance from the top wall to the location of U_M is y_M, whereas the distance from the bottom wall to the location of U_M is y_C (Fig. 3b). Both distances are made non-dimensional using the length L. The z-component of the vorticity is a useful quantity to characterize the flow in the vertical midplane (z/L = 0.5), and is defined as $\omega_z = (\partial v/\partial x) - (\partial u/\partial y)$, which is made dimensionless using the inlet height h and the maximum local velocity U_M as $\omega_z' = \omega_z h/U_M$.

3. Qualitative flow information

To ensure that the PIV measurements are conducted for Re-values in the transitional regime, flow visualizations were performed to obtain qualitative information on the flow pattern. A solution of fluorescein in water was injected into the flow field in the vertical center plane (z/L = 0.5) (Fig. 4a). A slide projector was installed above the test section to illuminate the fluorescent solution. An analysis of the flow pattern was made using recordings on video and photo camera, both devices were positioned perpendicular to the vertical center plane.

Flow visualizations were performed for Re ranging from 300 to 3,700. Figures 4(b-d) show instantaneous images of flow in the vertical center plane for Re ≈ 1,000, 1,750 and 2,500. For these Re-values, a transitional flow regime is observed. The presence of coherent structures is clearly visible in Figure 4b (Re ≈ 1,000). Although the presence of large-scale vortical structures in the outer region of the jet becomes less clear due to an increase of turbulence, they can still be distinguished for Re-values of 1,750 and 2,500 (Fig. 4c,d). The observed large-scale vortices are the result of the free shear layer that is situated in the outer region of the wall jet. From

these flow visualizations it can be concluded that transitional flow is present for Re up to at least 2,500. Therefore, PIV measurements were conducted for Re ranging from 800 to 2,500.

4. PIV measurement set-up

The PIV measurements were conducted using a 2D PIV system consisting of a Nd:Yag (532 nm) double-cavity laser (2 x 200 mJ, repetition rate < 10 Hz) to illuminate the field of view, and a CCD (Charge Coupled Device) camera (1376 x 1040 pixel resolution, max. 10 frames/s) for image acquisition. The laser was mounted on a translation stage and was positioned above the cubic test section to create a laser sheet in the vertical center plane (z/L = 0.5). The CCD camera was positioned perpendicular to the laser sheet plane (Fig. 5). Seeding of the water was provided by hollow glass micro spheres (3M; type K1) with diameters in the range of 30 – 115 μm.

In order to determine reliable time-averaged flow quantities, sufficient statistically-independent (uncorrelated) samples (i.e. PIV vector fields resulting from double image pairs) had to be acquired. Therefore, the PIV image acquisition frequency has to be sufficiently low. The required measuring frequency was estimated from the integral length scale (= inlet height h) and the characteristic velocity (i.e. inlet velocity U_0) and was set to 2 Hz. Each measurement set consisted of 360 uncorrelated samples, resulting in a sampling time of 180 seconds. The best practice guidelines of Prasad [74] were taken into account to minimize the systematic uncertainty of the PIV measurements. More information on PIV measurements can be found in Adrian and Westerweel [75].

Two sets of PIV measurements were performed in the vertical center plane of the test section. The first set concerns the entire cross-section of the cube, i.e. a region of interest (ROI) of L x L (Fig. 5; ROI1). The second set is focused on a smaller region of interest of 0.6L x 0.4L (W x H) in the proximity of the inlet to be able to measure with a higher spatial measuring resolution (Fig. 5; ROI2). This provides more detailed information in this area with expected large velocity gradients as a result of the boundary layer and shear layer flows. This type of information concerning the inlet conditions is important to determine the boundary conditions for future numerical simulations.

5. PIV measurement results

5.1 Time-averaged velocity vector fields

Figure 6 shows time-averaged velocity vector fields for Re values of 1,000, 1,750 and 2,500 and for the two regions of interest. Figures 6(a,c,e) show the large recirculation cell in the cube, which is driven by the jet. In addition, two smaller recirculation cells are distinguished in the upper right corner and the lower left corner. The flow pattern for these three Re-values appears to be almost identical. Figures 6(b,d,f) show the velocity vectors in the close vicinity of the inlet. Figure 6b shows a small recirculation cell near the inlet and below the jet, which becomes smaller with increasing Re (Fig. 6d) and cannot be distinguished for Re ≈ 2,500 (Fig. 6f). The Coanda effect cannot be clearly distinguished in these vector fields due to the fact that only 1 out of 4 vectors, in both x- and y-direction, is depicted. Therefore profiles of important flow properties will be presented in the next subsections.

5.2 Time-averaged velocity profiles near the inlet

Figure 7 shows vertical profiles of U/U_M obtained from the PIV measurements in ROI2 at three different downstream locations: x/L = 0.07, x/L = 0.27 and x/L = 0.47. Figure 7a seems to indicate that the differences between the profiles for the different Re-values are most pronounced below the jet and are relatively small. However, Figures 7(d,e) show that a top-hat profile is present at x/L = 0.07 for the lower Re-values, while the profile develops to a nearly parabolic profile with increasing Re. This is associated with an increasing thickness of the boundary layer and a decrease of the width of the potential core w_p (for which $U_M = U_0$). Figure 8a shows the width of the potential core (w_P/L) at x/L = 0.07, indicating a decrease in w_P/L with increasing Re. Figure 8b depicts the boundary layer thickness δ/L at x/L = 0.07, indicating the location where $U/U_M = 0.99$. At this location, the boundary layer thickness increases with increasing Re.

Below the jet (y/L < 0.9) the values of U/U_M increase with increasing Re (Figs. 7a-c). Figure 7a shows that for Re < 1,200, U/U_M is negative for 0.84 < y/L < 0.90, indicating the presence of the small recirculation cell near the bottom of the jet. Figure 7b shows the profiles of U/U_M at x/L = 0.27. At this location the differences in the inner region of the jet are still small, but the differences in the outer region have increased. At y/L = 0.9, U/U_M for Re ≤ 1,200 is around 0.2, while for Re ≥ 1,500 it lies around 0.4. At x/L = 0.47 (Fig. 7c), the profiles show a clear Re-dependency in both the inner and the outer region of the jet. In the inner region the location of

maximum jet velocity (y_C/L) approaches the top wall with increasing values of Re at x/L = 0.47. In the outer region the values of U/U_M are again higher for higher Re-values, as was observed in Figure 7b.

Figure 9 shows the development of the jet in the test section for Re ≈ 1,000, Re ≈ 1,750 and Re ≈ 2,500. From Figures 9(a-c) it can be observed that the location of maximum jet velocity (y_C/L; gray circles in Fig. 9(a-c)) increases after the jet was issued into the enclosure. This phenomenon is widely known in building engineering as the 'Coanda effect' and can be attributed to the lower pressure between the jet and the top surface of the enclosure resulting from the entrainment of ambient fluid by the jet [62-64]. Due to the Coanda effect the initially free jet develops into an attached wall jet (Fig. 9d). For Re ≈ 1,000 and Re ≈ 1,750 the highest value of y_C/L is present at x/L = 0.27, while for Re ≈ 2,500 the highest value is present at x/L = 0.47 (Fig. 9). Further downstream, y_C/L starts to decrease, indicating the spread of the wall jet. The jet center lines ($U/U_M = 1$) are depicted in Figures 9(a-c) as dashed lines, clearly illustrating the deflection of the jet towards the top surface.

5.3 Time-averaged turbulence profiles near the inlet

Vertical distributions of the longitudinal turbulence intensities u_{RMS}/U_M and vertical turbulence intensities v_{RMS}/U_M at x/L = 0.07, x/L = 0.27 and x/L = 0.47 are shown in Figure 10. Close to the inlet (x/L = 0.07) the profiles and values of u_{RMS}/U_M and v_{RMS}/U_M are quite similar (Figs. 10a,d), which is in agreement with the general profiles of turbulence intensities in free jets as reported in literature (e.g. [76,77]). The maximum values of u_{RMS}/U_M and v_{RMS}/U_M are located at y/L ≈ 0.92 and y/L ≈ 0.98, which are the locations that correspond with the shear layers of the jet at x/L = 0.07. Further downstream the differences between u_{RMS}/U_M and v_{RMS}/U_M become larger due to the development of the free jet into an attached wall jet. The profiles of u_{RMS}/U_M at x/L = 0.27 and x/L = 0.47 have two maxima, one at y/L ≈ 0.92 and one at y/L ≈ 0.99, which are the locations where the velocity gradients are large due to the shear layer and the boundary layer, respectively. In contrast, v_{RMS}/U_M has only one maximum at x/L = 0.27 and x/L = 0.47, namely at y/L ≈ 0.92, which corresponds to the position of the shear layer of the attached wall jet. Note that large differences are present for both the longitudinal and vertical turbulence intensities between Re ≤ 1,200 and Re ≥ 1,500 at x/L = 0.07 (Figs. 10a,d). Apparently, the turbulence level close to the inlet experiences a sudden increase for Re-values above Re ≈ 1,200.

The values of longitudinal turbulence intensity u_{RMS}/U_M and vertical turbulence intensity v_{RMS}/U_M below y/L = 0.8 are not depicted in this paper; these values remain fairly constant and fairly Re-independent, and are in the range of 0.03-0.04.

5.4 Time-averaged vorticity profiles near the inlet

Figure 11 shows the vertical profiles of the dimensionless z-vorticity (ω_z') at x/L = 0.27 and x/L = 0.47. In the jet region, the positive and negative values of ω_z' indicate the inner and outer region of the jet, with dU/dy < 0 and dU/dy > 0, respectively. It is shown that ω_z' is larger in the boundary layer than in the shear layer at both locations, which is the result of the larger velocity gradients (dU/dy) in the former compared to the latter (see Figs. 7b,c). Figure 11a shows that there is no clear Re-dependency at x/L = 0.27, the profiles of ω_z' are almost overlapping. At x/L = 0.47 (Fig. 11b), the profiles show some differences for different values of Re. However, no clear tendency can be found. At both locations, slightly negative values of ω_z' are present below the jet (y/L < 0.85), indicating the clockwise rotating recirculation cell in the cube. These slightly negative values below y/L = 0.85, $\omega_z' \approx -0.05$ at x/L = 0.27 and $\omega_z' \approx -0.08$ at x/L = 0.47, continue in the region below ROI2 and extend all the way down to the low-velocity wall jet at the bottom of the cube.

5.5 Time-averaged velocity profiles in the entire flow domain

Figures 12a-c show vertical profiles of U/U_M at x/L = 0.2, 0.5 and 0.8. These profiles clearly indicate the jet at the top of the enclosure and the large recirculation zone with low velocities that is driven by the jet. Note that the profiles are not shown for y/L < 0.05 since the measurement results in this part of the cube are inaccurate due to reflections of the laser sheet on the glass bottom of the cube. The following observations are made:

- Figure 12a: At x/L = 0.2, the jet occupies the region between y/L = 0.9 and 1. For y/L between 0.8 and 0.9, a locally lower velocity U/U_M is present. Below y/L = 0.8, U/U_M shows an almost linear decrease to values around $U/U_M = -0.2$ at y/L = 0.1. U/U_M reaches zero somewhere between y/L = 0.4 and 0.5. In the area 0.1 < y/L < 0.9, a Re-number dependency is present.
- Figure 12b: At x/ L = 0.5, the jet region has extended down to about y/L = 0.87. Below y/L = 0.87, the large recirculation cell is present, where U/U_M reaches zero at about y/L = 0.5. In the recirculation cell, there is a clear Re-number dependency of U/U_M: the absolute value of U/U_M increases with increasing Re-values.

- Figure 12c: At x/L = 0.8, the jet region has extended down to about y/L = 0.7. Below y/L = 0.7, the velocity ratio U/U_M ranges from about 0.1 to -0.1. U/U_M is zero at about y/L = 0.5. Re-number dependency is less pronounced than at x/L = 0.2 and 0.5. Note that at x/L = 0.8, Re-number dependency is larger in the jet region than in the recirculation cell.

6. Discussion

Experimental results of forced mixing ventilation driven by a transitional plane jet have been presented in this paper. A reduced-scale set-up filled with water was used to perform flow visualizations and PIV measurements. The flow visualizations have revealed a transitional flow regime for slot Reynolds numbers from 800 to 2,500; therefore PIV measurements were conducted for the same range of Re-values.

To the knowledge of the authors, experimental work as presented in this paper is quite scarce. Although previous publications indicated the importance and difficulties in modeling transitional ventilation flow, the vast majority of experiments on room airflow were conducted for fully turbulent flow. Consequently, there is a lack of experimental data on transitional room airflow to validate numerical models. There are some limitations concerning the experimental work described in this paper.

- The reflections of the laser sheet on the glass bottom of the test section made it impossible to analyze the flow in this area of the cube. As a result, some information on the flow pattern is lacking, although one must note that the bottom of the cube is not the primary area of interest in this study, in contrast to the wall jet region. Future studies focused on flow near the bottom of the cube will use a non-reflective paint.
- The turbulence intensity was accurately measured in ROI2, providing enough information on the turbulence intensities in the jet region for validation purposes. However, these measurements do not allow identifying the reason for the strong increase in turbulence intensities for Re > 1,200, that was observed just downstream of the inlet. Additional measurements in the inlet area could provide more information concerning this observation. Unfortunately, the current design of the experimental set-up does not allow for measurements upstream of the inlet.
- The current PIV measurements were performed with a temporal resolution of 2 Hz, which does not classify as time-resolved PIV. Future work should consist of measurements with a higher temporal resolution to collect time-resolved PIV data for the detailed validation of Large Eddy Simulation (LES).

This study is a first step in a more extensive research project on forced mixing ventilation driven by transitional jets. Future work will include measurements for additional inlet opening heights h/L, different inlet geometries and additional values of the slot Reynolds number $Re = U_0 h/\nu$. In addition to the PIV measurements, point measurements will be conducted in an air filled set-up (2 x 2 x 2 m^3) using Laser Doppler Anemometry. These point measurements will provide time-resolved data of the airflow pattern, which will provide valuable complementary information to the data set presented in this paper, and will be beneficial for the validation of unsteady CFD simulations (e.g. Large Eddy Simulation).

7. Conclusions

This paper presents PIV measurements and analysis of transitional flow in a ventilated enclosure. An experimental set-up has been designed to study forced mixing ventilation driven by a transitional plane jet. Flow visualizations have been performed to identify the Re-range for which transitional flow occurs. Based on the results of the flow visualizations, PIV measurements have been conducted for seven Re-values, ranging from 800 to 2,500. The time-averaged velocities, vorticity and the turbulence intensities are presented in this paper and can be used to develop and validate CFD models.

The following conclusions can be made:

- The flow visualizations indicated that a transitional flow regime is present for Re-values ranging from 800 to 2,500.
- For all tested Re values (800-2,500), the time-averaged velocity vector field shows the jet near the ceiling of the enclosure that drives a large recirculation cell, with smaller recirculation zones below the jet inlet and in the top right and bottom left corner. The size of the small recirculation cell below the jet decreases with increasing Re.
- The time-averaged velocity profiles show a clear Re dependency; this dependency increases with increasing distance from the inlet.
- The Coanda effect causes the free plane jet to transform in a wall jet just downstream of the inlet.
- The location of maximum jet velocity (y_C/L) depends on Re; y_C/L increases with increasing Re.

- After attachment of the jet, the turbulence intensity profiles transform from typical free jet turbulence intensity profiles to typical wall jet turbulence intensity profiles.
- The longitudinal turbulence intensities are higher in the boundary layer and the shear layer. The vertical turbulence intensities (after attachment of the jet) have a maximum in the shear layer and decrease with increasing y/L as a result of the boundary layer flow.
- The longitudinal and vertical turbulence intensities below the jet region are in the same order of magnitude and are around 0.03-0.04. No clear Re-dependency is present.
- The large velocity gradients in the inner and outer region of the wall jet due to the boundary layer and the shear layer result in increased values of positive and negative z-vorticity, respectively. The z-vorticity is higher in the boundary layer than in the shear layer as a result of a higher velocity gradient in the boundary layer. The dimensionless z-vorticity shows no clear Re-dependency. The weak negative vorticity in the center of the test section is associated with the large clockwise-rotating recirculation cell.

8. Acknowledgements

Twan van Hooff is currently a PhD student funded by both Eindhoven University of Technology in the Netherlands and Fonds Wetenschappelijk Onderzoek (FWO) - Flanders, Belgium (FWO project number: G.0435.08). The FWO Flanders supports and stimulates fundamental research in Flanders. Its contribution is gratefully acknowledged. Thijs Defraeye is a postdoctoral fellow of the FWO – Flanders and acknowledges its support.

The measurements reported in this paper were supported by the Laboratory of the Unit Building Physics and Services (BPS) at Eindhoven University of Technology and the Laboratory of Building Physics at the Katholieke Universiteit Leuven. Special thanks go to Jan Diepens, head of LBPS, and Wout van Bommel, Harrie Smulders and Geert-Jan Maas, members of the LBPS, for their valuable contributions.

9. References

[1] Chen Q. Ventilation performance prediction for buildings: A method overview and recent applications. Build Environ 2009;44:848-58.
[2] Linden PF. The fluid mechanics of natural ventilation. Annu Rev Fluid Mech 1999;31:201-38.
[3] Coffey CJ, Hunt GR. Ventilation effectiveness measures based on heat removal: Part 2. Application to natural ventilation flows. Build Environ 2007;42(6):2249-62.
[4] Ji Y, Cook MJ, Hanby V. CFD modelling of natural displacement ventilation in an enclosure connected to an atrium. Build Environ 2007;42(3):1158-72.
[5] Cockroft JP, Robertson P. Ventilation of an enclosure through a single opening. Build Environ 1976;11:29–35.
[6] Crommelin RD, Vrins EMH. Ventilation through a single opening in a scale model. Air Infilt Rev 1988;9(3):11-5.
[7] Allocca C, Chen Q, Glicksman LR. Design analysis of single-sided natural ventilation, Energy Build 2003;35(8):785-95.
[8] Larsen TS, Heiselberg P. Single-sided natural ventilation driven by wind pressure and temperature difference. Energy Build 2008;40(6):1031-40.
[9] Nielsen PV. Flow in air conditioned rooms, PhD Thesis, Technical University of Denmark, Copenhagen 1974.
[10] Nielsen PV. Specification of a two-dimensional test case. International Energy Agency, Energy Conservation in Buildings and Community Systems, Annex 20: Airflow Pattern within Buildings; 1990.
[11] Kato S, Murakami S, Mochida A, Akabayashi A, Tominaga Y. Velocity-pressure field of cross ventilation with open windows analyzed by wind tunnel and numerical simulation. J Wind Eng Ind Aerodyn 1992;44:2575-86,
[12] Hunt GR, Linden PF. The fluid mechanics of natural ventilation - displacement ventilation by buoyancy-driven flows assisted by wind. Build Environ 1999;34(6):707-20.
[13] Straw MP, Baker CJ, Robertson AP. Experimental measurements and computations of the wind-induced ventilation of a cubic structure. J Wind Eng Ind Aerodyn 2000;88(2-3):213-30.
[14] Ohba M, Irie K, Kurabuchi T. Study on airflow characteristics inside and outside a cross-ventilation model, and ventilation flow rates using wind tunnel experiments. J Wind Eng Ind Aerodyn 2001;89(14-15):1513-24.

[15] Jiang Y, Alexander D, Jenkins H, Arthur R, Chen Q. Natural ventilation in buildings: Measurement in a wind tunnel and numerical simulation with large-eddy simulation. J Wind Eng Ind Aerodyn 2003;91(3): 331-53.
[16] Karava P, Stathopoulos T, Athienitis AK. Wind-induced natural ventilation analysis. Solar Energy 2007;81:20-30.
[17] Norton T, Grant J, Fallon R, Sun D-W. Assessing the ventilation effectiveness of naturally ventilated livestock buildings under wind dominated conditions using computational fluid dynamics. Biosystems Eng 2009;103(1):78-99.
[18] Karava P, Stathopoulos T, Athienitis AK. Airflow assessment in cross-ventilated buildings with operable façade elements. Build Environ 2011;46:266-79.
[19] Zhang G, Morsing S, Bjerg B Svidt K, Strøm JS. Test room for validation of airflow patterns estimated by computational fluid dynamics. J Agric Eng Res 2000;76:141-48.
[20] Yang T, Wright NG, Etheridge DW, Quinn AD. A comparison of CFD and full-scale measurements for analysis of natural ventilation. Int J Vent 2006;4(4):337-48.
[21] Gao NP, Niu JL, Perino M, Heiselberg P. The airborne transmission of infection between flats in high-rise residential buildings: tracer gas simulation. Build Environ 2008;43(11):1805–17.
[22] Wang M, Chen Q. Assessment of various turbulence models for transitional flows in enclosed environment. HVAC&R Res 2009;15:1099-1119.
[23] Wang M, Chen Q. On a hybrid RANS/LES approach for indoor airflow modelling. HVAC&R Res 2010;16:731-747.
[24] Van Hooff T, Blocken B. Coupled urban wind flow and indoor natural ventilation modelling on a high-resolution grid: A case study for the Amsterdam ArenA stadium. Environ Modell Softw 2010;25(1):51-65.
[25] Rundle CA, Lightstone MF, Oosthuizen P, Karava P, Mouriki E. Validation of computational fluid dynamics simulations for atria geometries. Build Environ 2011;46:1343-53.
[26] Magnier L, Zmeureanu R, Derome D, Experimental assessment of the velocity and temperature distribution in an indoor displacement ventilation jet. Build Environ 2012;47:150-60.
[27] Wang L, Chen Q. Evaluation of some assumptions used in multizone airflow network models. Build Environ 2008;43(10):1671–77.
[28] Wang L, Chen Q. Theoretical and numerical studies of coupling multizone and CFD models for building air distribution simulations. Indoor Air 2007;17(5):348–61.
[29] Firrantello J, Bahnfleth WP, Musser A, Freihaut JD, Jeong J-W. Use of factorial sensitivity analysis in multizone airflow model tuning. ASHRAE Trans 2007;113:642–51.
[30] Inard C, Bouia H, Dalicieux P. Prediction of air temperature distribution in buildings with a zonal model. Energy Build 1996;24:125–32.
[31] Rees SJ, Haves P. 2001. A nodal model for displacement ventilation and chilled ceiling systems in office spaces. Build Environ 2001;36:753–62.
[32] Voeltzel A, Carrie FR, Guarracino G. Thermal and ventilation modelling of large highly-glazed spaces. Energy Build 2001;33:121–32.
[33] Song F, Zhao B, Yang X, Jiang Y, Gopal V, Dobbs G, Sahm M. A new approach on zonal modeling of indoor environment with mechanical ventilation. Build Environ 2008;43(13):278-86.
[34] Jiang Y, Chen Q. Effect of fluctuating wind direction on cross natural ventilation in buildings from large eddy simulation. Build Environ 2002;37(4):379-86.
[35] Cook MJ, Ji Y, Hunt GR. CFD modeling of natural ventilation: combined wind and buoyancy forces. Int J Vent 2003;1(3):169-80.
[36] Heiselberg P, Li Y, Andersen A, Bjerre M, Chen Z. Experimental and CFD evidence of multiple solutions in a naturally ventilated building. Indoor Air 2004;14(1):43–54.
[37] Wright NG, Hargreaves DM. Unsteady CFD simulations for natural ventilation. Int J Vent 2006;5(1):13-20.
[38] Yang T, Wright NG, Etheridge DW, Quinn AD. A comparison of CFD and full-scale measurements for analysis of natural ventilation. Int J Vent 2006;4(4):337-48.
[39] Hu C-H, Ohba M, Yoshie R. CFD modelling of unsteady cross ventilation flows using LES. J Wind Eng Ind Aerodyn 2008;96(10-11):1692-1706.
[40] Horan JM, Finn DP. Sensitivity of air change rates in a naturally ventilated atrium space subject to variations in external wind speed and direction. Energy Build 2008;40(8):1577-85.
[41] Teitel M, Ziskind G, Liran O, Dubovsky V, Letan R. Effect of wind direction on greenhouse ventilation rate, airflow patterns and temperature distributions. Biosystems Eng 2008;101(3):351-69.
[42] Norton T, Grant J, Fallon R, Sun D-W. Assessing the ventilation effectiveness of naturally ventilated livestock buildings under wind dominated conditions using computational fluid dynamics. Biosystems Eng 2009;103(1):78-99.

[43] van Hooff T, Blocken B, On the effect of wind direction and urban surrounding on natural ventilation of a large semi-enclosed stadium. Comput Fluids 2010;39: 1146-55.
[44] van Hooff T, Blocken B, Aanen L, Bronsema B. A venturi-shaped roof for wind-induced natural ventilation of buildings: wind tunnel and CFD evaluation of different design configurations. Build Environ 2011;46(9):1797-1807.
[45] Blocken B, van Hooff T, Aanen L, Bronsema B. Computational analysis of the performance of a venturi-shaped roof for natural ventilation: venturi-effect versus wind-blocking effect. Comput Fluids 2011;48(1):202-13.
[46] Ramponi R, Blocken B. CFD simulation of cross-ventilation for a generic isolated building: impact of computational parameters. Build Environ 2012;53:34-48.
[47] Chen Q. Comparison of different k-ε models for indoor airflow computations. Numer Heat Tr B-Fund 1995;28:353-69.
[48] Chen Q. Prediction of room air motion by Reynolds-stress models. Build Environ 1996;31:233-44.
[49] Nielsen PV. The selection of turbulence models for prediction of room airflow. ASHRAE T 1998;104(1B):1119-27.
[50] Nielsen PV, Restivo A, Whitelaw JH. The velocity characteristics of ventilated rooms. Trans ASME, J Fluids Eng 1978;100: 291–8.
[51] Li Y, Nielsen P. CFD and ventilation research. Indoor Air 2011;21:442-53.
[52] Casey M, Wintergerste T (Eds). Best Practice Guidelines, ERCOFTAC Special Interest Group on Quality and Trust in Industrial CFD, ERCOFTAC, Triomflaan 43, B-1160, Brussels; 2000.
[53] Chen Q, Srebric J. How to verify, validate, and report indoor environment modeling CFD analyses. Final Report for ASHRAE RP-1133, 58 pages, Welsh School of Architecture, Cardiff University, UK and Department of Architectural Engineering, Pennsylvania State University, PA; 2001.
[54] Srebric J. Chen Q. An example of verification, validation, and reporting of indoor environment CFD analyses. ASHRAE Trans 2002;108(2):185-94.
[55] Chen Q, Srebric J. A procedure for verification, validation, and reporting of indoor environment CFD analyses. HVAC&R Res 2002;8(2):201-16.
[56] Franke J, Hellsten A, Schlünzen H, Carissimo B (Eds.). Best practice guideline for the CFD simulation of flows in the urban environment. COST Office Brussels; 2007.
[57] Franke J, Hirsch C, Jensen AG, Krüs HW, Schatzmann M, Westbury PS, Miles SD, Wisse JA, Wright NG. Recommendations on the use of CFD in wind engineering. In: van Beeck, J.P.A.J. (Ed.), COST Action C14, Impact of Wind and Storm on City Life Built Environment, Proceedings of the International Conference on Urban Wind Engineering and Building Aerodynamics. Von Karman Institute, Sint-Genesius-Rode, Belgium, 5–7 May 2004.
[58] Tominaga Y, Mochida A, Yoshie R, Kataoka H, Nozu T, Yoshikawa M, Shirasawa T. AIJ guidelines for practical applications of CFD to pedestrian wind environment around buildings. J Wind Eng Ind Aerod 2008;96(10-11): 1749-61.
[59] Blocken B, Stathopoulos T, Carmeliet J, Hensen JLM. Application of CFD in building performance simulation for the outdoor environment: an overview. J Build Perform Simul 2011;4(2):157184.
[60] Blocken B, Janssen, WD, van Hooff T. CFD simulation for pedestrian wind comfort and wind safety in urban areas: General decision framework and case study for the Eindhoven University campus. Environ Modell Software 2012; 30:15-34.
[61] Sørensen DN, Nielsen PV. Quality control of computational fluid dynamics in indoor environments. Indoor Air 2003;13:2–17.
[62] Awbi HB. Ventilation systems: design and performance. London: Taylor & Francis; 2007.
[63] Etheridge DW, Sandberg M. Building Ventilation: Theory and Measurement. London: Wiley; 1996.
[64] Awbi HB. Ventilation of buildings. London: Spon Press; 2003.
[65] Topp C, Nielsen PV, Davidson L. Room airflows with low Reynolds number effects. Proc. of Roomvent 2000, Oxford, 541-46; 2000.
[66] Nielsen PV, Filholm C, Topp C, Davidson L. Model experiments with low Reynolds number effects in a ventilated room. Proc. of Roomvent 2000, Oxford, 185-90; 2000.
[67] Davidson L, Nielsen PV, Topp C, 2000. Low Reynolds number effects in ventilated rooms: a numerical study. Proc. of Roomvent 2000, Oxford, 307-12; 2000.
[68] van Hooff T, Blocken B, Defraeye T, Carmeliet J, van Heijst GJF. PIV measurements of a plane wall jet in a confined space at transitional slot Reynolds numbers. Submitted.
[69] Bradshaw P. The effect of wind tunnel screens on nominally two-dimensional boundary layers. J Fluid Mech 1965;22:679-87.
[70] Groth J, Johansson AV. Turbulence reduction by screens. J Fluid Mech 1988;197:139-55.
[71] Bell JH, Mehta RD. Contraction design for small low-speed wind tunnels. NASA CR-177488; 1988.

[72] Brassard D, Ferchichi M. Transformation of a polynomial for a contraction wall profile. J Fluids Eng 2005;127:183-85.
[73] Defraeye T. Design of a vertical wind tunnel for heat and mass transfer coefficients. M.Sc. thesis. Laboratory of Building Physics, Department of Civil Engineering, K.U.Leuven; 2006.
[74] Prasad AK. Particle image velocimetry. Curr Sci 2000;79:51-60.
[75] Adrian RJ, Westerweel J. Particle Image Velocimetry. New York: Cambridge University Press; 2011.
[76] Quinn WR, Militzer J, Effects of nonparallel exit flow on round turbulent free jets. Int J Heat Fluid Flow 1989;10(2):139-45.
[77] Deo RC, Mi J, Nathan GJ. The influence of Reynolds number on a plane jet. Phys Fluids 2008;20:075108.

FIGURES

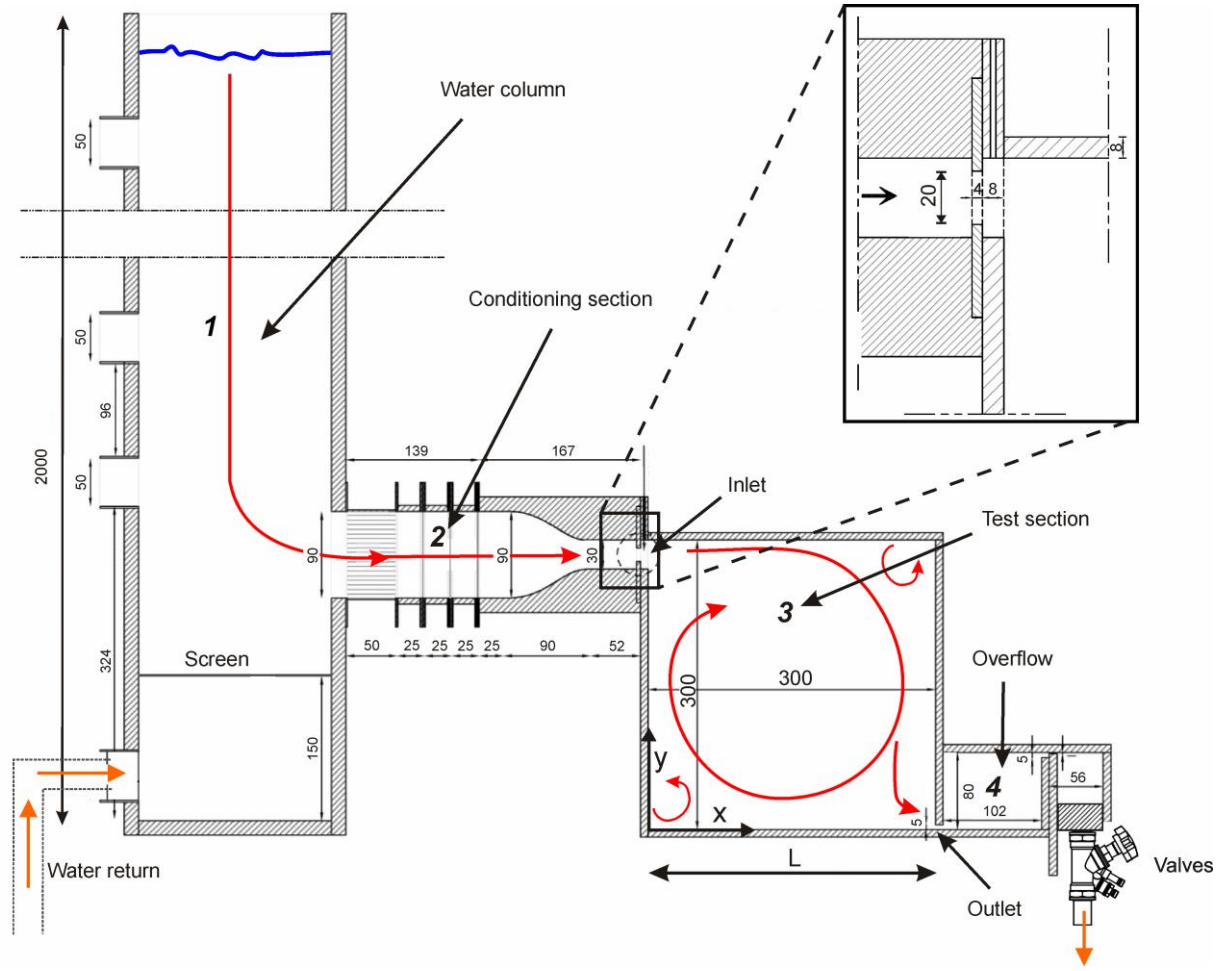

Fig. 1: Reduced-scale set-up for the flow visualizations and PIV measurements: (1) water column; (2) flow conditioning section in front of the inlet, (3) test section, (4) overflow, and the valves that are placed in a block downstream of the overflow. Dimensions in mm.

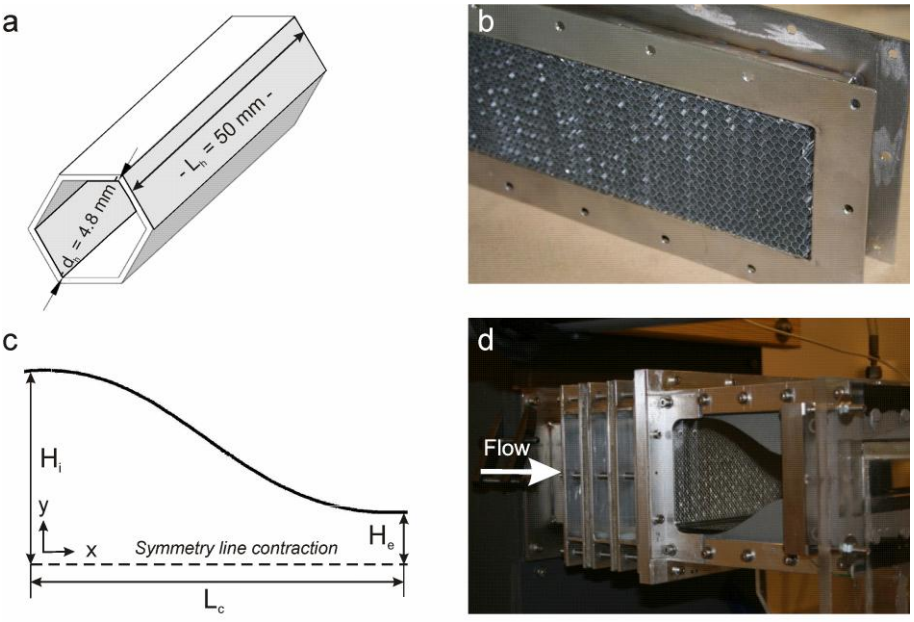

Fig. 2: (a) Honeycomb geometry: d_h = 4.8 mm, L_h = 50 mm. (b) Picture of honeycomb. (c) Illustration of the contraction indicating the parameters H_i, H_e, L_c. (d) Conditioning section of the reduced-scale set-up. The contraction and one of the screens can be distinguished.

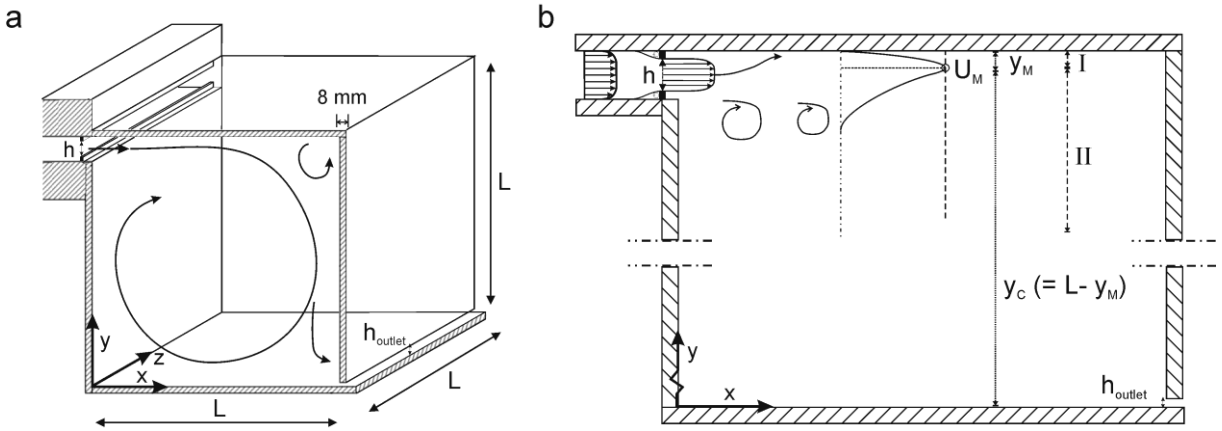

Fig. 3: (a) 3D representation of the test section of the experimental set-up, depicting the coordinate system, the inlet height h, the outlet height h_{outlet} and the dimensions of the test section L^3. (b) 2D schematic representation of the plane jet with I the inner region, II the outer region, U_M the maximum velocity, y_M the distance from the top wall to the location of U_M and y_C the distance from the bottom wall to the location of U_M.

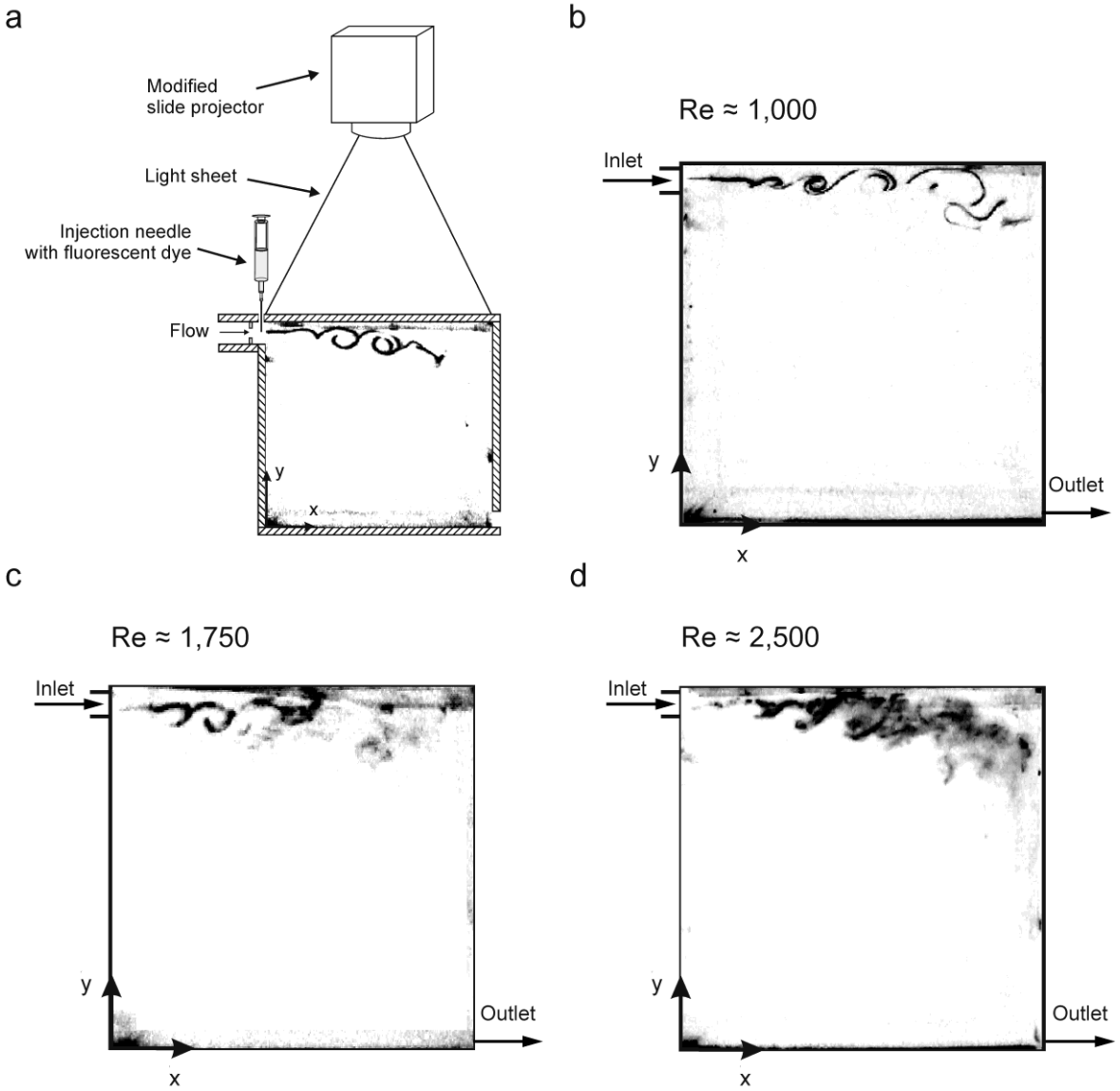

Fig. 4: (a) Overview of the reduced-scale set-up during flow visualizations. (b,c,d) Instantaneous images of the flow pattern in the vertical center plane of the enclosure for h/L = 0.067 and for three different Re-values; Re ≈ 1,000 (b); Re ≈ 1,750 (c); Re ≈ 2,500 (d).

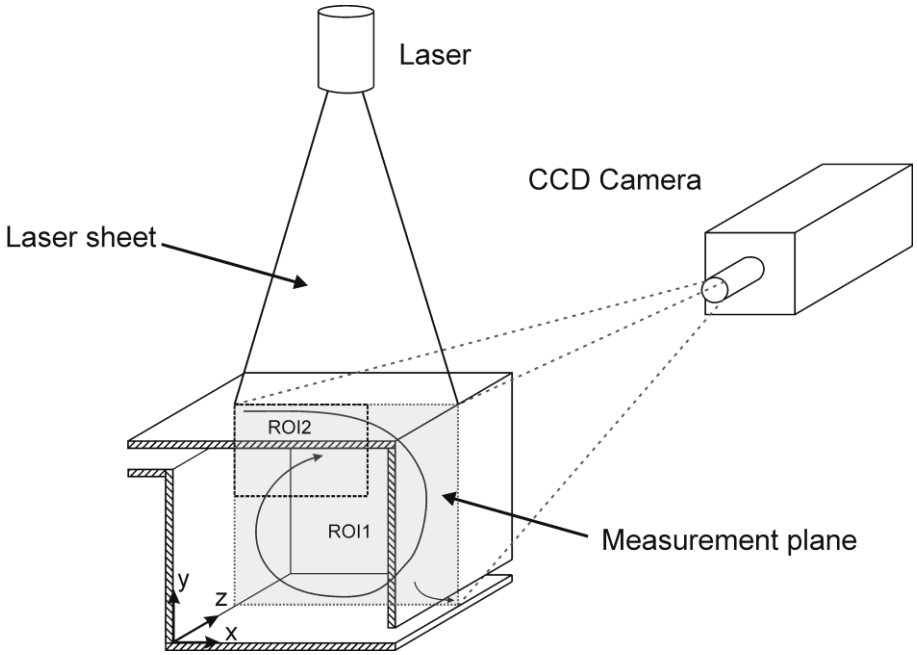

Fig. 5: PIV measurement set-up; the laser head is positioned above the test section using a translation stage. The measurement planes are indicated with ROI1 and ROI2; ROI1 indicates the region of interest (L x L) for the first measurement set, ROI2 indicates the region of interest of 0.6L x 0.4L (W x H) for the second measurement set.

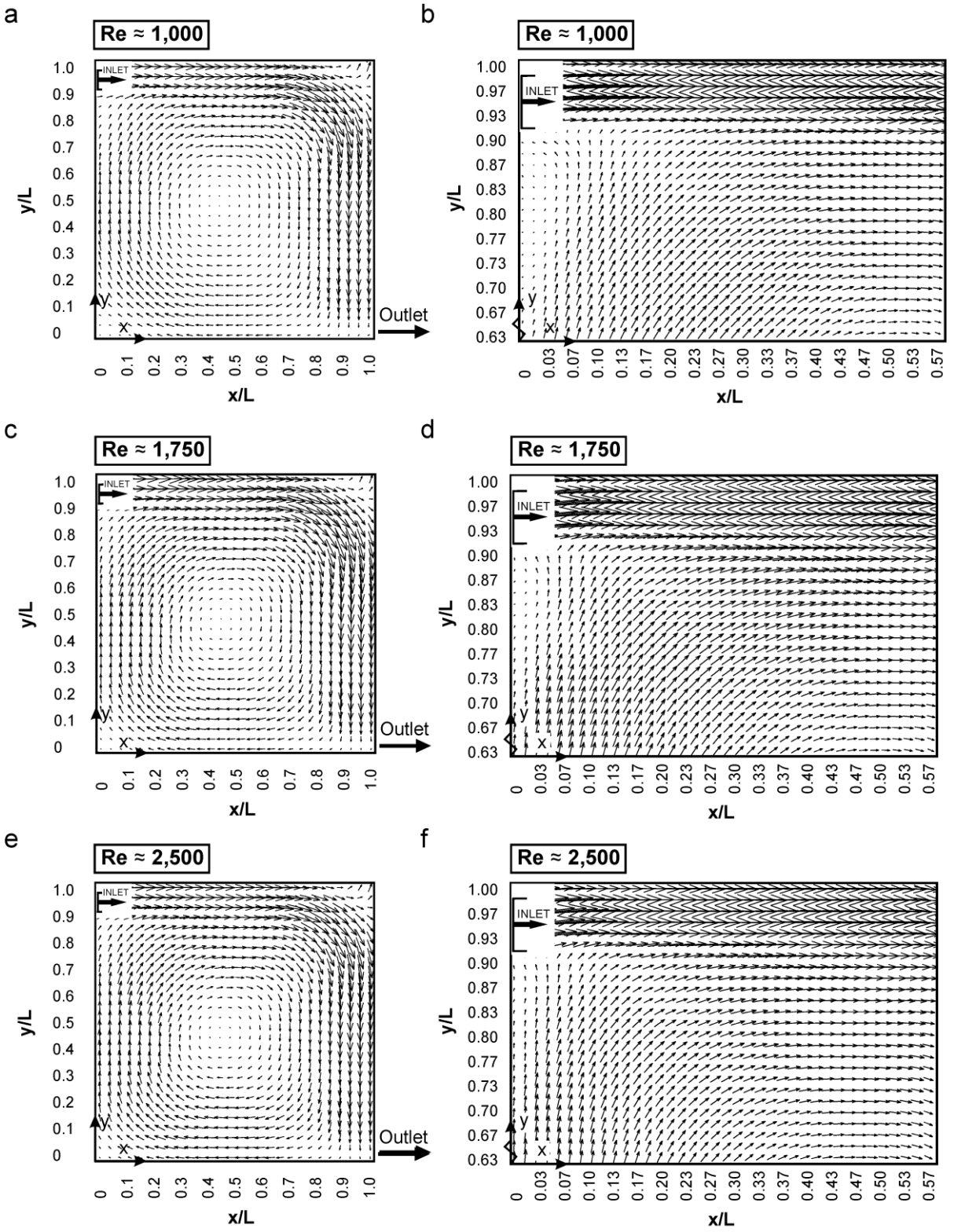

Fig. 6: Time-averaged velocity vector fields for Re ≈ 1,000 (a,b), Re ≈ 1,750 (c,d), Re ≈ 2,500 (e,f). Note that only 1 out of 4 vectors is shown in all figures; i.e. the actual resolution is sixteen times higher than shown. The velocity vectors are scaled with Re and velocity vectors in the close vicinity of the inlet are omitted; due to reflections at the walls the reliability of these vectors could not be guaranteed. (a,c,e) Measurements for entire cross-section (ROI1); (b,d,f) measurements with a higher spatial resolution near the inlet (ROI2).

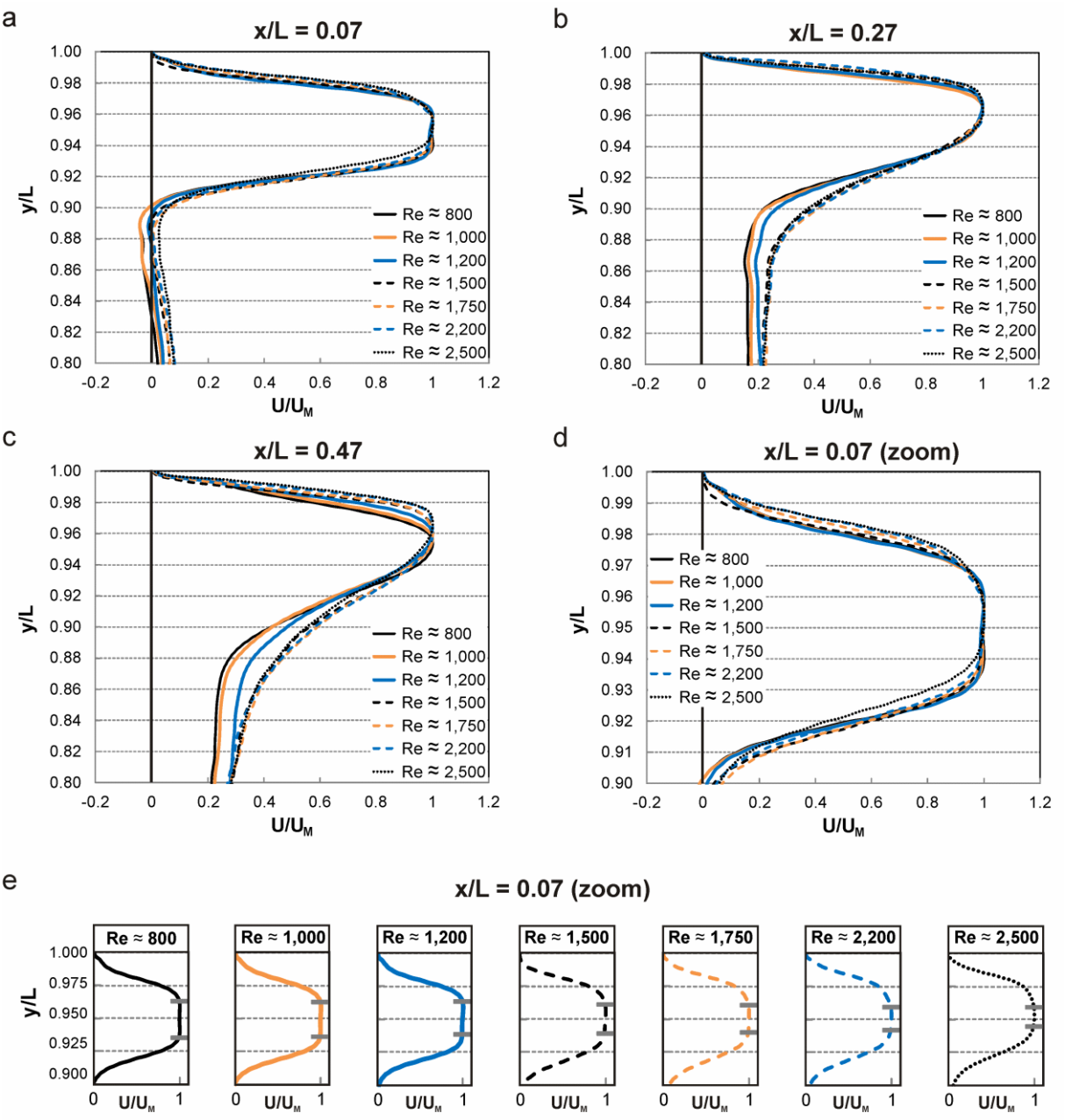

Fig. 7: Time-averaged vertical profiles of U/U_M at x/L = 0.07 (a), x/L = 0.27 (b), x/L = 0.47 (c). Panel (d) presents an enlarged view of U/U_M at x/L = 0.07. Panel (e) shows the transformation from a top-hat profile to a nearly parabolic profile and the decrease of the potential core and increase of the boundary layer thickness with increasing Re-values.

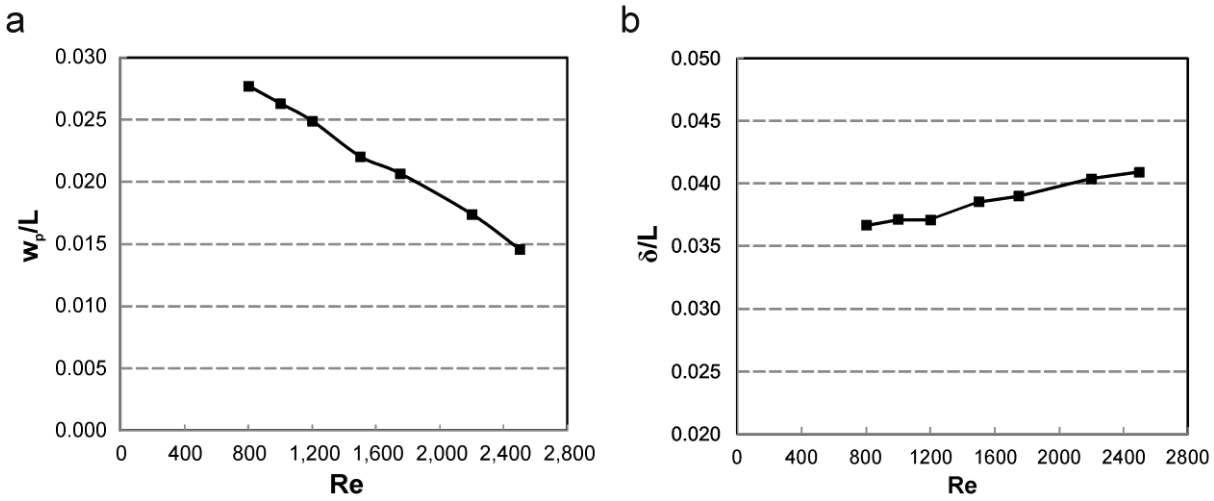

Fig. 8: (a) Width of the potential core w_p/L as function of Re. (b) Boundary layer thickness δ/L as function of Re. Both are taken at x/L = 0.07.

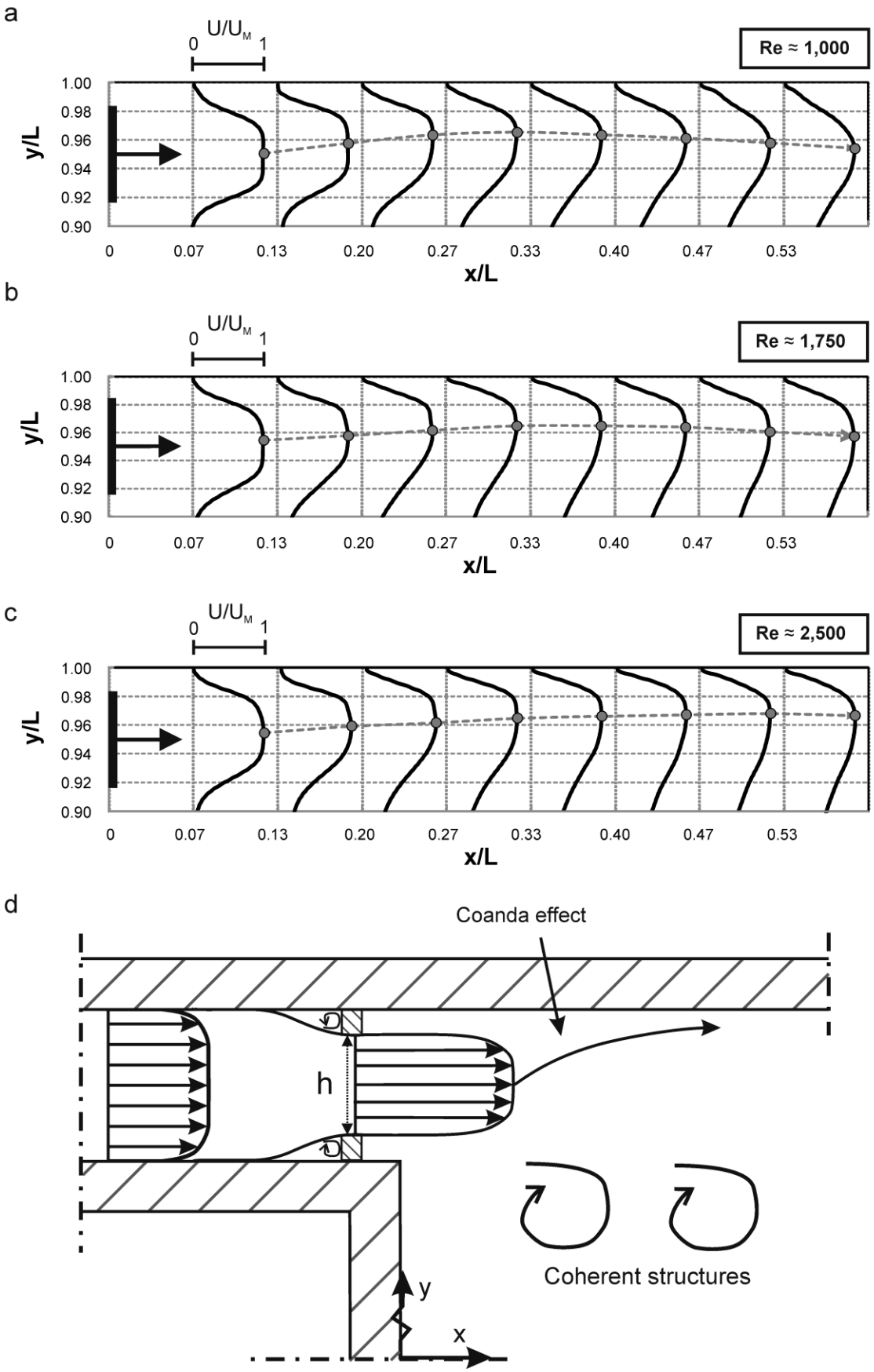

Fig. 9: Time-averaged vertical profiles of U/U_M to illustrate the jet development and the Coanda effect for (a) Re ≈ 1,000; (b) Re ≈ 1,750; (c) Re ≈ 2,500. (d) Schematic representation of the flow near the inlet. Downstream of the inlet the Coanda effect deflects the jet towards the top surface.

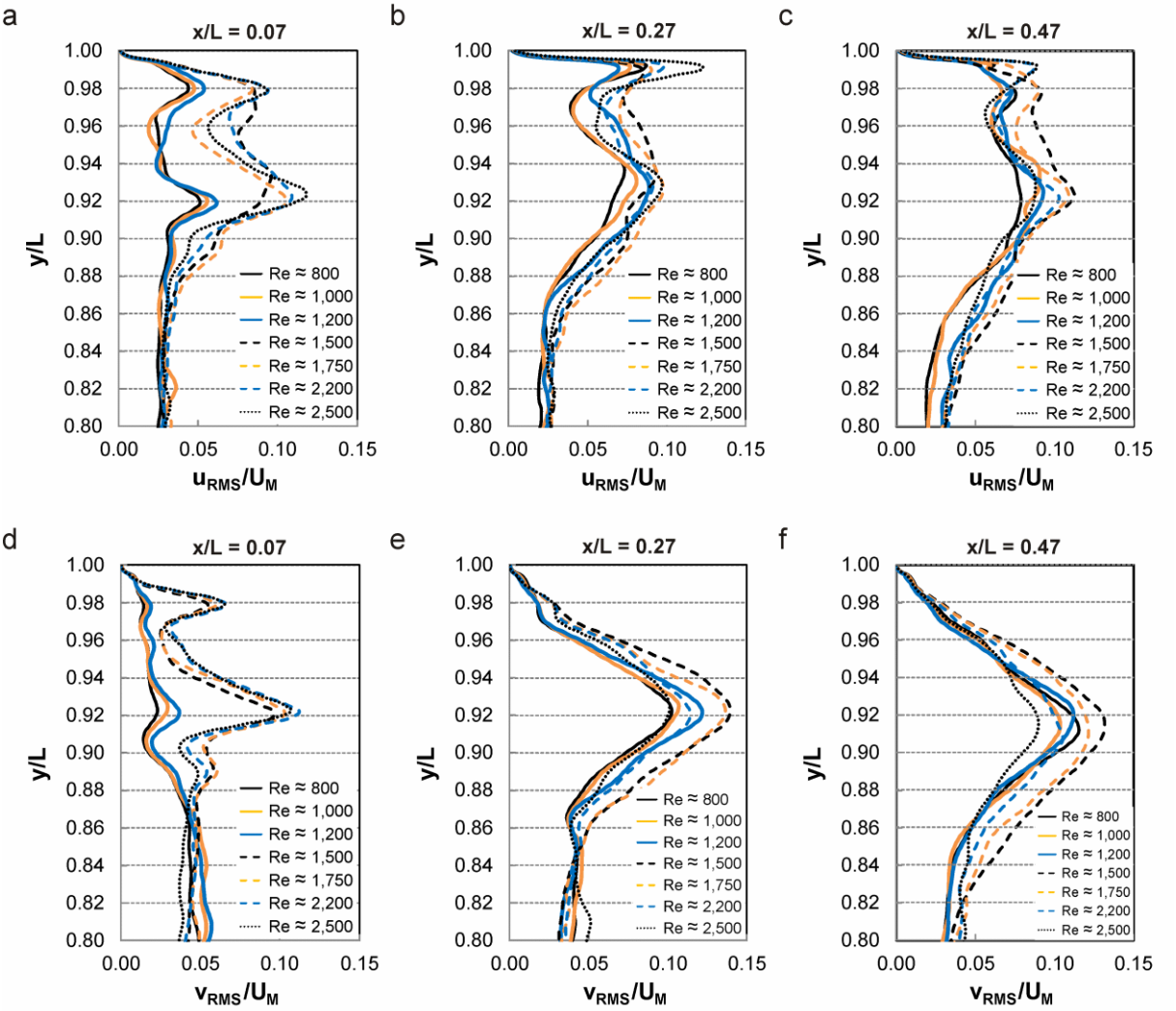

Fig. 10: Time-averaged vertical profiles of longitudinal turbulence intensity (u_{RMS}/U_M) (a,b,c) and vertical turbulence intensity (v_{RMS}/U_M) (d,e,f) at x/L = 0.07 (a,d), x/L = 0.27 (b,e), x/L = 0.47 (c,f).

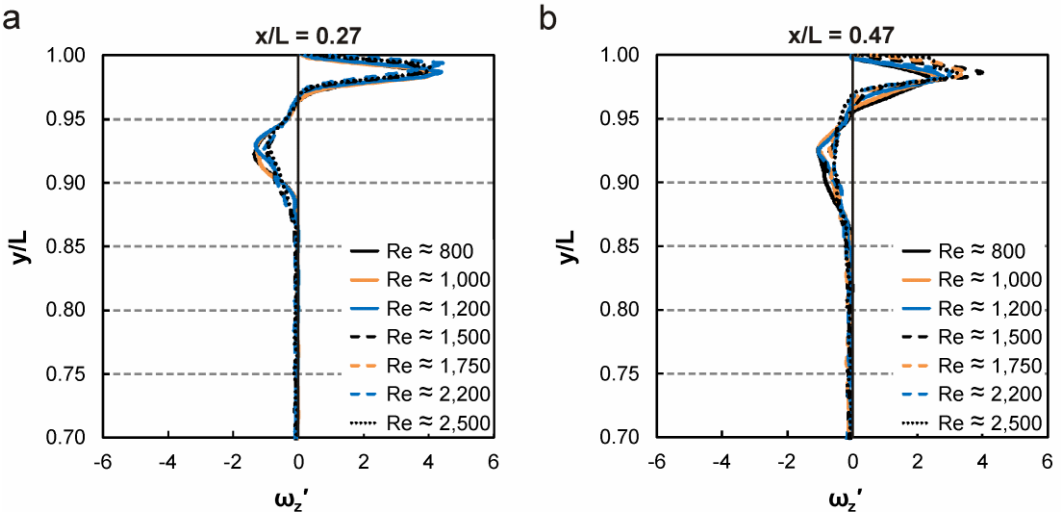

Fig. 11: Time-averaged vertical profiles of dimensionless z-vorticity ω_z' at x/L = 0.27 (a), x/L = 0.47 (b).

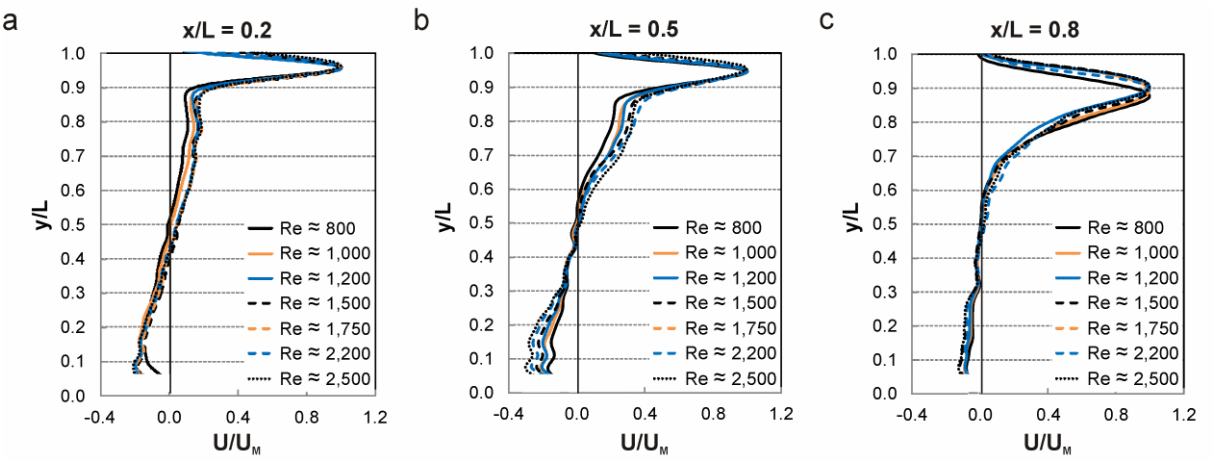

Fig. 12: Time-averaged vertical profiles of U/U_M at x/L = 0.2 (a), x/L = 0.5 (b), x/L = 0.8 (c).